One Coordination Cage, Many Pathways: Multiple Stimuli Drive Reversible Transformations

Romain Guechaichia, Amina Benchohra, Liam Miller, Jennifer Bou Zeid, David Canevet, Magali Allain, Vincent Carré, Frédéric Aubriet, Luca Pesce, Denis Jacquemin, et al.

JACS Au
AN OPEN ACCESS JOURNAL OF THE AMERICAN CHEMICAL SOCIETY

pubs.acs.org/jacsau
Article

One Coordination Cage, Many Pathways: Multiple Stimuli Drive Reversible Transformations

Romain Guechaichia, Amina Benchohra, Liam Miller, Jennifer Bou Zeid, David Canevet, Magali Allain, Vincent Carré, Frédéric Aubriet, Luca Pesce,* Denis Jacquemin,* Marc Sallé,* and Sébastien Goeb*

Cite This: https://doi.org/10.1021/jacsau.6c00216
Read Online

ACCESS | Metrics & More | Article Recommendations | Supporting Information

ABSTRACT: A trigonal prismatic coordination cage endowed with a large cavity is built by self-association of a bis(rhodium) complex and a planar triazatruxene-based ligand. The remarkable versatility of this molecular building in promoting reversible structural transformations is demonstrated through manipulating three orthogonal external stimuli, i.e., cage concentration, guest identity, and pH. Four distinct stable discrete structures can be formed on-demand: a monomeric cage, two distinct host–guest complexes, and a mechanically interlocked cage dimer, and all these structures are fully and readily interconvertible. The cage uniquely couples (i) selective double guest encapsulation, (ii) stimulus-controlled reversible catenation, and (iii) pH-triggered pairwise guest release-uptake. The resulting structures were comprehensively characterized using 1D and 2D NMR spectroscopy, high-resolution mass spectrometry, theoretical calculations, and, in most cases, single-crystal X-ray diffraction.

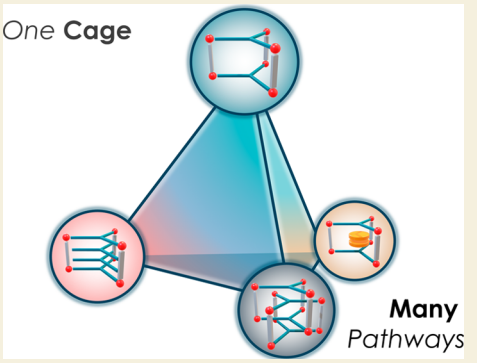

KEYWORDS: *self-assembly, coordination cages, stimuli-induced transformations, pH, triazatruxene*

INTRODUCTION

Metal–organic cages constitute a class of discrete supramolecular architectures formed through coordination-driven self-assembly of metal ions and organic ligands.[1−7] These well-defined three-dimensional structures feature cavities that can potentially encapsulate guest molecules,[2,6] with applications in catalysis,[8−12] molecular separation,[13−16] drug delivery,[5,17−19] and materials science[20,21] to cite a few. Their structural flexibility has motivated an intense interest in stimuli-responsive architectures, for which an external input is able to modify the host's geometry, composition, or guest-binding properties.[22−28]

In analogy to biological systems, where proteins and other biomolecules adapt their structure and function in response to multiple external signals, coordination cages can undergo controlled transformations upon application of chemical or physical stimuli. Changes in pH,[29−31] redox state,[32−35] guest binding,[36−40] light irradiation,[41−45] solvent polarity, or concentration[46−49] have all been used to trigger reversible modifications of cage geometry, composition, or guest-binding behavior.

In most reported examples, however, such responsiveness is limited to relatively simple binary transitions between two discrete states. As a result, coordination cages capable of accessing multiple distinct structures in a controlled and reversible manner, while remaining addressable by orthogonal stimuli, remain comparatively rare. Achieving this level of complexity requires that several structurally and functionally distinct states be selectively stabilized under different conditions without compromising the integrity of the assembly or leading to uncontrolled mixtures. Recent studies have approached the case of multiple external inputs that are combined to navigate between different cage architectures, highlighting the potential of such systems to display pathway-dependent behavior and emergent properties.[50−64] Nevertheless, examples in which several transformations are coherently integrated within a single coordination cage are still limited.

Herein, we report a trigonal prismatic $(\mathbf{Rh_2})_3\mathbf{L_2}$ cage based on a planar π-rich triazatruxene ligand **L** and bis(rhodium) $\mathbf{Rh_2}$ panels that addresses these challenges simultaneously. The corresponding spacious cavity is able to bind two planar guests or alternatively to generate a mechanically interlocked cage dimer. Importantly, this system is designed to respond to three orthogonal stimuli (i.e., cage concentration, guest formula, or pH), affording a tetrahedral network of reversible structural transformations (Figure 1). Depending on the input, three discrete systems can be produced on-demand from the monomeric cage $(\mathbf{Rh_2})_3\mathbf{L_2}$, i.e., two distinct host–guest

Received: February 10, 2026
Revised: April 16, 2026
Accepted: April 16, 2026
Published: April 30, 2026

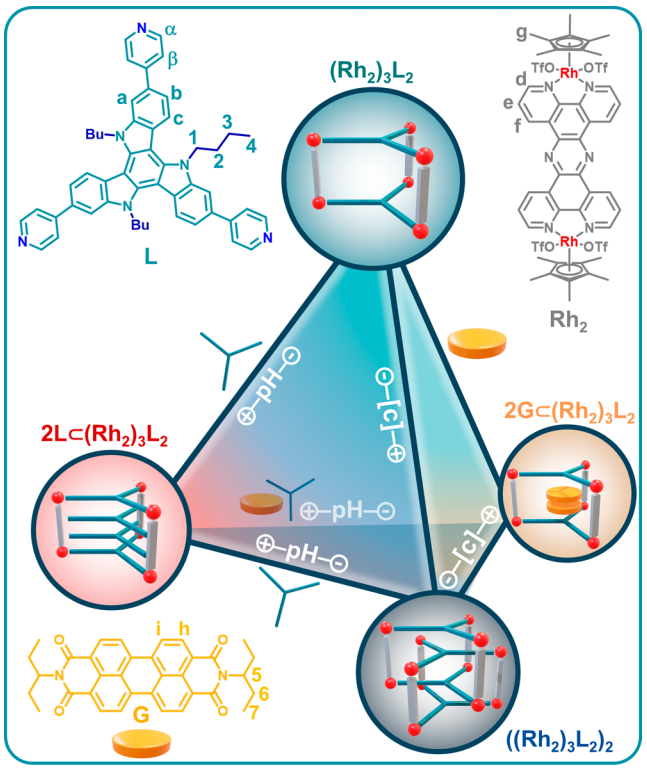

Figure 1. Representation of ligand **L**, panel $\mathbf{Rh_2}$, and the four interconvertible states arising from the self-assembled $(\mathbf{Rh_2})_3\mathbf{L_2}$ cage through application of various stimuli. The ligand **L** is represented in its anticlockwise face "A"-oriented toward the viewer, see Figure S1 for details.

complexes ($\mathbf{2L}\subset(\mathbf{Rh_2})_3\mathbf{L_2}$ and $\mathbf{2G}\subset(\mathbf{Rh_2})_3\mathbf{L_2}$) or a triply interlocked dimer $((\mathbf{Rh_2})_3\mathbf{L_2})_2$. All four states are cleanly and reversibly connected without cage decomposition. All these interchangeable structures have been thoroughly characterized using 1D and 2D NMR spectroscopy, mass spectrometry, and, in most cases, X-ray diffraction analyses. In parallel to the experimental characterization, complementary insights into the structural preferences of the system were reached using classical Molecular Dynamics (MD) simulations along with enhanced sampling simulations to evaluate the relative stability of representative stereoisomers, the guest dynamics, and the effect of interlocking.[65,66]

RESULTS AND DISCUSSION

Ligand **L**, derived from the triazatruxene platform, was synthesized and fully characterized as described in the Supporting Information. It combines C_3-symmetry with a fully planar, electronically delocalized π-surface. In contrast to truxene analogues,[67−69] the sp^2-hybridized nitrogen bridges rigidify the core and increase its π-acidity, while preserving two distinct faces, denoted as "C" and "A" (i.e., clockwise and anticlockwise rotation, respectively), originating from the orientation of the N−*n*Bu substituents (Figure S1). Although **L** is achiral, this facial differentiation enables stereochemical discrimination within self-assembled architectures.

Single crystals of **L** were obtained by vapor diffusion of methyl *tert*-butyl ether into a dichloromethane solution of the ligand and analyzed by single-crystal X-ray diffraction (Figures 2a, S73, and S74). In the crystal, the ligand molecules are arranged as interacting pairs with an interplanar distance of 3.7 Å. Two crystallographically independent pairs are present in the asymmetric unit, corresponding to mixtures of CA and AC pairs. Within each pair, the ligands adopt a slightly twisted arrangement, characterized by a Bailar angle of 16°.[17]

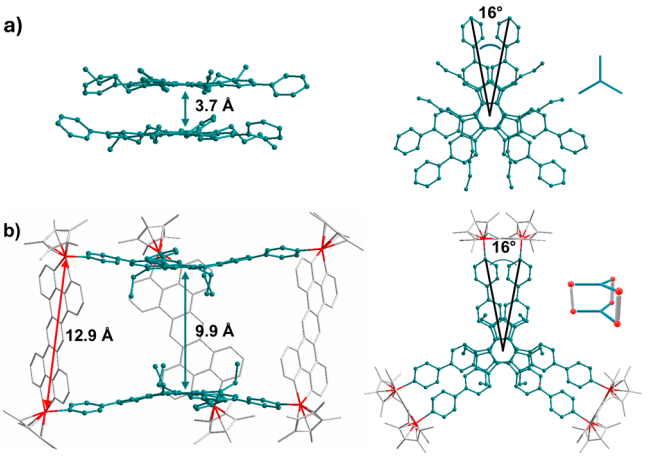

Figure 2. X-ray crystal structures of (a) ligand **L** and (b) cage $(\mathbf{Rh_2})_3\mathbf{L_2}$.

Synthesis and Characterizations of Cage $(Rh_2)_3L_2$

The self-assembly between ligand **L** and complex $\mathbf{Rh_2}$ was achieved in nitromethane-d_3 ($C = 10^{-3}$ M) at 50 °C. High-resolution ESI-FTICR mass spectrometry analyses (Figures 3a and S18), as well as ^{1}H Diffusion Ordered Spectroscopy (DOSY) NMR analyses (Figures 4a and S15−S17) reveal the formation of a single M_6L_2 species with a diffusion coefficient of $D = 2.3 \times 10^{-10}$ $m^2 \cdot s^{-1}$. This corresponds to a hydrodynamic radius of $R = 16$ Å, in accordance with the

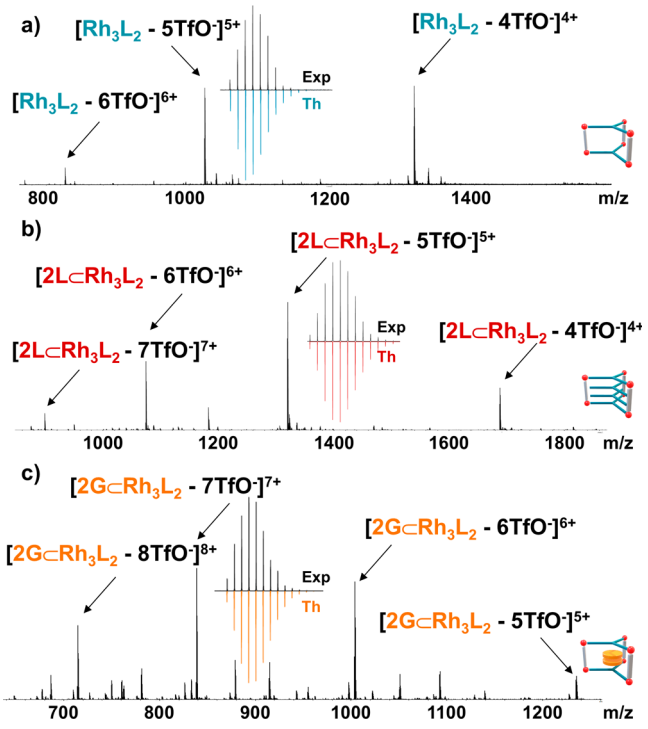

Figure 3. ESI-FTICR high-resolution mass spectrometry spectra recorded in nitromethane for (a) $(\mathbf{Rh_2})_3\mathbf{L_2}$, (b) $\mathbf{2L}\subset(\mathbf{Rh_2})_3\mathbf{L_2}$, and (c) $\mathbf{2G}\subset(\mathbf{Rh_2})_3\mathbf{L_2}$. For each spectrum, one experimental isotopic pattern is compared with the simulated one.

https://doi.org/10.1021/jacsau.6c00216
JACS Au XXXX, XXX, XXX−XXX

diameter D = 32 Å observed in the solid state.[70] The ^{1}H NMR spectrum shows a well-defined set of resonances with a doubling of the butyl-chain signals, particularly for the terminal methyl group "4". This reflects the coexistence of two stereochemically distinct cage species arising from the relative facial orientations of the two **L** ligands. Although four formal combinations can be drawn (CC, AA, CA, and AC), symmetry considerations reduce these to two NMR-distinguishable species: an achiral CC/AA form and a chiral CA/AC pair (Figure S1). The comparable intensities indicate a statistical distribution, consistent with the large separation between the two ligands, which minimizes intramolecular stereochemical communication.

Single crystals suitable for X-ray diffraction were obtained by vapor diffusion of methyl *tert*-butyl ether into a nitromethane solution of cage $(\mathbf{Rh_2})_3\mathbf{L_2}$. The solid-state structure (Figures 2b, S75 and S76) confirms the formation of a trigonal prismatic $(\mathbf{Rh_2})_3\mathbf{L_2}$ assembly, in which two nearly planar triazatruxene ligands are connected by three $\mathbf{Rh_2}$ units. The cage displays a large, unobstructed cavity with a ligand−ligand separation of ca. 10 Å and only a modest geometric distortion. Whereas in solution the full set of stereoisomers is present, only the CA/AC arrangement is observed in the crystal (Figure S76). This solid-state selection may therefore reflect packing or solubility effects during crystallization rather than a strong thermodynamic preference in solution. Computations nonetheless identify CA/AC as a low-energy arrangement (Table S2). Overall, the structure reveals a rigid open cavity suitable for binding planar guests or generating interlocked assemblies.

Binding Properties of Cage $(\mathbf{Rh_2})_3\mathbf{L_2}$. The binding properties of $(\mathbf{Rh_2})_3\mathbf{L_2}$ were examined using two different planar molecules: an electron-poor perylenediimide (PDI) derivative **G** chosen for its electronic complementary with the electron-rich walls of the cavity and compound **L**, used in the construction of cage $(\mathbf{Rh_2})_3\mathbf{L_2}$, selected for its geometric matching with the cavity components (Figures 4 and S19−S30). In both cases, addition of the guest molecules in nitromethane-d_3 induced significant chemical shift variations in the ^{1}H NMR spectra (Figure 4b,c), indicative of strong $\pi-\pi$ interactions within the cavity. The exchange behavior differs for the two guests: whereas the binding equilibrium is slow on the ^{1}H NMR time scale in the case of **L**, with distinct signals for the free and bound cages, compound **G** leads to a fast exchange, manifested by a gradual evolution of the cage resonances. Adding more than two equiv of substrates **L** and **G** had no further impact on the NMR signatures, suggesting that two guest molecules occupy the cavity. Since both **L** and **G** are only sparingly soluble in nitromethane, they remain as suspensions once the cage is saturated, and their excess does not give rise to any detectable signals. ^{1}H DOSY NMR spectroscopies were run in nitromethane-d_3 at a concentration of 10^{-3} M (Figure 4b,c). In both cases, a single diffusion coefficient, similar to that of the empty cage (Figure 4a), was observed for the host and guest, indicating the formation of the host−guest complexes without significant structural expansion of the host structure.

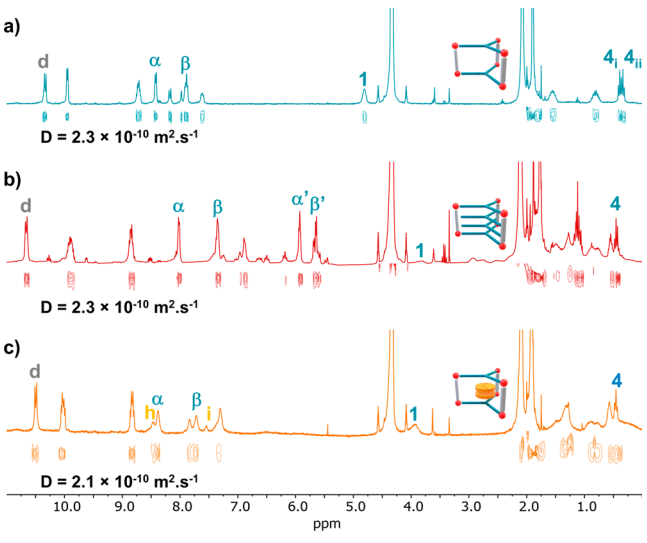

Figure 4. ^{1}H NMR spectra (nitromethane-d_3, C = 10^{-3} M, 298 K) of (a) $(\mathbf{Rh_2})_3\mathbf{L_2}$, (b) $(\mathbf{Rh_2})_3\mathbf{L_2}$ in the presence of 2 equiv of **L**, and (c) $(\mathbf{Rh_2})_3\mathbf{L_2}$ in the presence of 2 equiv of **G**. Assignment of protons is provided in Figures S19 and S27. Primed labels (′) correspond to protons of the encapsulated guest, whereas unprimed labels correspond to protons of the cage framework.

A 1:2 host−guest binding was established by ESI-FTICR mass spectrometry analyses recorded in nitromethane (Figures 3b,c, S22 and S30), which reveals the exclusive presence of signals arising from the $\mathbf{2L}\subset(\mathbf{Rh_2})_3\mathbf{L_2}$ and $\mathbf{2G}\subset(\mathbf{Rh_2})_3\mathbf{L_2}$ complexes. The preferential formation of the 1:2 complexes arises from the size and geometry of the $(\mathbf{Rh_2})_3\mathbf{L_2}$ cage, whose elongated π-rich cavity can accommodate two aromatic guests simultaneously. In contrast, the inclusion of a single guest would result in incomplete filling of the cavity and weaker overall interactions. Accordingly, no evidence of 1:1 complexes could be detected by either NMR or mass spectrometry.

Several experiments were carried out to explore the potential for the simultaneous encapsulation of both **L** and **G** within the cavity. A mixture of the cage with **L** (one equivalent) and **G** (one equivalent) led exclusively to the separate formation of $\mathbf{2L}\subset(\mathbf{Rh_2})_3\mathbf{L_2}$ and $\mathbf{2G}\subset(\mathbf{Rh_2})_3\mathbf{L_2}$ as shown by ^{1}H NMR (Figure S32c) and ESI-FTICR mass spectrometry (Figure S34). No signal attributable to a mixed complex involving simultaneous **L** and **G** binding was detected, revealing a pronounced preference for narcissistic encapsulation. The exclusive formation of homoleptic host−guest complexes can be rationalized by geometric factors. The trigonal prismatic cavity of $(\mathbf{Rh_2})_3\mathbf{L_2}$ provides two symmetrical binding sites, and the encapsulation of two identical guests leads to optimal packing while maximizing the stabilizing host−guest interactions. In contrast, a mixed complex containing two different guests would result in less efficient packing within the confined cavity and is therefore disfavored.

To assess the competitive binding of **L** and **G**, the cage $(\mathbf{Rh_2})_3\mathbf{L_2}$ was next exposed to two equivalents of each guest in nitromethane-d_3 at $C = 10^{-3}$ M. It is worth noting that under the experimental conditions used, both guests **L** and **G** exhibit limited solubility in the nitromethane-based solvent systems and are, therefore, initially present as suspensions. The ^{1}H NMR analysis (Figure S32d) reveals the exclusive formation of $\mathbf{2L}\subset(\mathbf{Rh_2})_3\mathbf{L_2}$ while **G** remains suspended as a solid, which indicates a stronger affinity of $(\mathbf{Rh_2})_3\mathbf{L_2}$ for **L** vs **G**. This observation is also supported by the computational models that show stronger binding of both guest molecules in $\mathbf{2L}\subset(\mathbf{Rh_2})_3\mathbf{L_2}$, compared to $\mathbf{2G}\subset(\mathbf{Rh_2})_3\mathbf{L_2}$ (Table S1).

X-ray diffraction of a single crystal of $\mathbf{2L}\subset(\mathbf{Rh_2})_3\mathbf{L_2}$ obtained by vapor diffusion of iPr_2O into a nitromethane solution (Figures 5a, S77 and S78) shows that the two encapsulated ligands are perfectly stacked between the triazatruxene panels,

https://doi.org/10.1021/jacsau.6c00216
JACS Au XXXX, XXX, XXX−XXX

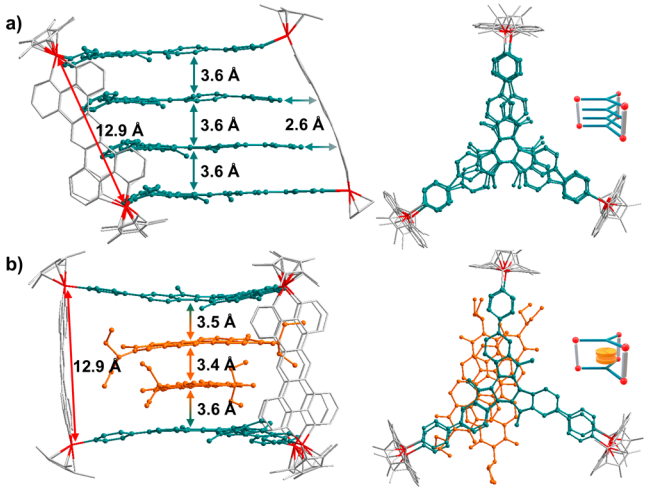

Figure 5. (a) X-ray crystal structure of $\mathbf{2L}\subset(\mathbf{Rh_2})_3\mathbf{L_2}$ and (b) MM^+ simulation of $\mathbf{2G}\subset(\mathbf{Rh_2})_3\mathbf{L_2}$.

generating a highly ordered four-layer π-stacking with uniform interplanar distances (~3.6 Å). Stabilizing N$-\pi^*$ contacts[71] with average distances of 2.6 Å between the pyridyl units of the guests and the cage's phenazine-based walls further reinforce the assembly. This arrangement is consistent with molecular simulations, which identify the experimentally observed CCAA/AACC configurations as the energetically preferred host–guest states (Table S2). The elongated cavity of the cage can accommodate two aromatic guests simultaneously. In the solid-state structures, the two guests are positioned within the cavity in close proximity, allowing favorable $\pi-\pi$ interactions in addition to host–guest interactions. Although guest binding may occur stepwise, no intermediate 1:1 complex is clearly observed in the NMR spectra, suggesting that the fully loaded 2:1 complex is the dominant species under the experimental conditions.

Synthesis and Characterizations of Interlocked Cages $((\mathbf{Rh_2})_3\mathbf{L_2})_2$

While numerous strategies exist for constructing macrocycles and coordination cages, the controlled assembly of mechanically interlocked architectures remains a significant challenge.[72−77] This arises from the progressive decrease in the number of independent species during the reaction, which is entropically unfavorable. Overcoming this limitation requires additional driving forces, e.g., $\pi-\pi$ interactions, electrostatic attractions, hydrogen bonding, or solvophobic effects. These factors can be modulated by fine-tuning several parameters such as the solvent composition, concentration, or temperature.[72−77] With this in mind, we proceeded with the self-assembly reaction between ligand **L** and $\mathbf{Rh_2}$ in a mixture of nitromethane-d_3 and acetonitrile-d_3 across a range of concentrations. Above $C = 5 \times 10^{-3}$ M (Figure S39), a new species appears, reaching exclusive formation at $C = 2 \times 10^{-2}$ M (Figures 6 and S35−S37). The corresponding ^{1}H NMR spectrum is significantly more complex than that of $(\mathbf{Rh_2})_3\mathbf{L_2}$, with several aromatic and aliphatic protons shifted upfield (up to $\delta = -2$ ppm for protons 4) (Figures 6c and S35). ^{1}H DOSY NMR reveals a single discrete species in solution with a unique diffusion coefficient of $D = 2.5 \times 10^{-10}$ m^2·s^{-1} (solvent mixture: acetonitrile-d_3 nitromethane-d_3 1:1 v/v) corresponding to a hydrodynamic radius of $R = 20$ Å, consistent with the formation of interlocked $((\mathbf{Rh_2})_3\mathbf{L_2})_2$ cages.[78] High-resolution

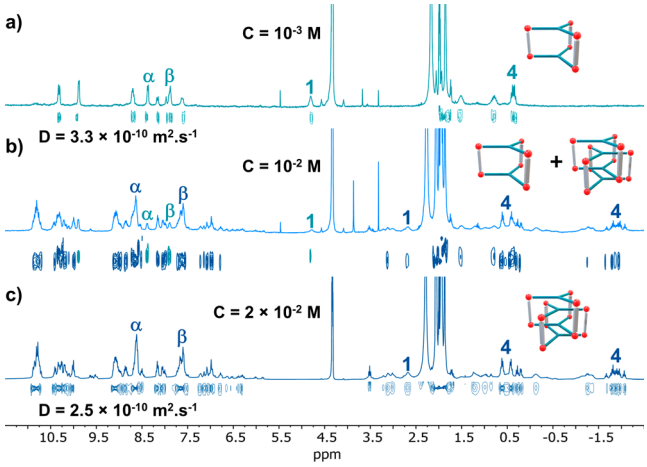

Figure 6. ^{1}H NMR spectra of a mixture of ligand **L** (2 equiv) and complex $\mathbf{Rh_2}$ (3 equiv) (nitromethane-d_3/acetonitrile-d_3, 298 K) at different concentrations: (a) $C = 10^{-3}$ M (cage $(\mathbf{Rh_2})_3\mathbf{L_2}$), (b) 10^{-2} M (cage $(\mathbf{Rh_2})_3\mathbf{L_2}$ and interlocked cages $((\mathbf{Rh_2})_3\mathbf{L_2})_2$), and (c) 2×10^{-2} M (interlocked cages $((\mathbf{Rh_2})_3\mathbf{L_2})_2$). Diagnostic signals for $(\mathbf{Rh_2})_3\mathbf{L_2}$ and $((\mathbf{Rh_2})_3\mathbf{L_2})_2$ in (b) are indicated above the spectra using schematic representations of the corresponding species. Assignment of protons is provided in Figure S35.

ESI-FTICR MS supports its assignment as a mechanically interlocked dimer (Figures 7a and S38).

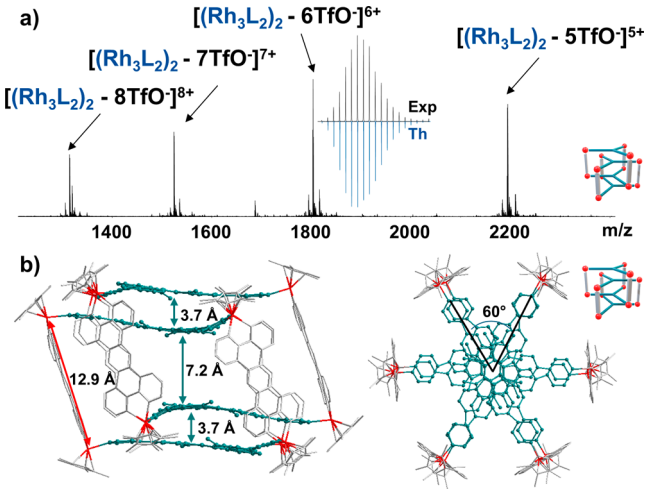

Figure 7. ESI-FTICR high-resolution mass spectrometry spectra recorded in nitromethane for $(\mathbf{Rh_2})_3\mathbf{L_2}$ (one experimental isotopic pattern is compared with the simulated one) and (b) X-ray crystal structure of the interlocked cages $((\mathbf{Rh_2})_3\mathbf{L_2})_2$.

The different shielding effects undergone by the butyl chains in the interlocked dimer $((\mathbf{Rh_2})_3\mathbf{L_2})_2$ and $\mathbf{2L}\subset(\mathbf{Rh_2})_3\mathbf{L_2}$ arise from their distinct structural arrangements. Whereas the four TAT units (**L**) are perfectly stacked in $\mathbf{2L}\subset(\mathbf{Rh_2})_3\mathbf{L_2}$, limiting interactions between the peripheral butyl chains and the aromatic surfaces of neighboring triazatruxene panels, interlocked dimer $((\mathbf{Rh_2})_3\mathbf{L_2})_2$ features a relative 60° rotation of the cages (vide infra). This spatial organization brings the butyl chains close to both the $\mathbf{Rh_2}$ units and the π-surfaces, resulting in pronounced upfield shifts below 0 ppm.

Finally, X-ray diffraction analysis from crystals obtained by slow evaporation of ethyl acetate into a solution of the interlocked cages in a 1:1 mixture of nitromethane/acetonitrile

https://doi.org/10.1021/jacsau.6c00216
JACS Au XXXX, XXX, XXX−XXX

unambiguously confirms the interlocked nature of the assembly. Several sets of crystals, obtained from independent crystallization experiments, were analyzed. In all cases, among the ten possible stereoisomeric combinations (Figure S2), only the CAAC/ACCA pair is observed (Figures 7b, S79 and S80), indicating a high degree of stereoselectivity. This organization is likely preferred to favor $\pi-\pi$ interactions between the triazatruxene platforms. The relative orientation of the two cages is offset by 60° (Figure S79), which minimizes the steric repulsion between the rhodium side panels. Interlocking also flattens the Rh−Rh axes and induces a slight distortion of the triazatruxene units while maintaining well-defined $\pi-\pi$ contact regions (intercage spacing ≈3.7 Å). In the computational model, we did not observe a significant energetic difference between CCAA and CAAC interlocked arrangements. This suggests that the formation of the dimer might occur through a kinetically preferred pathway.

The formation of the interlocked dimer[72] likely proceeds through concentration-dependent intermolecular association of two cage units, where the increased concentration enhances the probability of cage−cage encounters required for the threading process. The solid-state structure reveals multiple noncovalent interactions between the ligand frameworks and the $\mathbf{Rh_2}$ units, which likely contribute to the stabilization of the interlocked architecture. The slow interconversion observed between the monomeric cage and the interlocked dimer on the NMR time scale suggests the presence of a significant kinetic barrier associated with this threading process. In addition, the solvent composition, in particular, the use of acetonitrile, is expected to influence both the solvation of the cages and the balance of intermolecular interactions, thereby modulating the formation of the interlocked species.

In short, controlled access to either the monomeric cage structure $(\mathbf{Rh_2})_3\mathbf{L_2}$, the corresponding host−guest complexes $\mathbf{2L}\subset(\mathbf{Rh_2})_3\mathbf{L_2}$ and $\mathbf{2G}\subset(\mathbf{Rh_2})_3\mathbf{L_2}$ as well as the dimeric interlocked cages $((\mathbf{Rh_2})_3\mathbf{L_2})_2$ has been demonstrated, offering a unique opportunity to explore the adaptive and reconfigurable nature of these systems through their supramolecular transformations in response to external stimuli. The different assemblies can be readily distinguished by their characteristic ^{1}H NMR signatures. Guest encapsulation leads to pronounced shifts of the cage aromatic protons and of the guest resonances located inside the cavity, while the formation of the mechanically interlocked dimer gives rise to strongly shielded aliphatic signals.

Concentration-Induced Interconversion between the Dimeric Interlocked Cages $((Rh_2)_3L_2)_2$ and the Monomeric Cage $(Rh_2)_3L_2$

The interconversion between the interlocked dimer $((\mathbf{Rh_2})_3\mathbf{L_2})_2$ and the monomeric cage $(\mathbf{Rh_2})_3\mathbf{L_2}$ constitutes a representative example of the dynamic behavior displayed by this system. As shown above (Figure 6), concentrating the monomer solution in a nitromethane-d_3/acetonitrile-d_3 mixture (1/1 v/v) afforded the interlocked architecture. Conversely, we observed that refluxing a diluted solution of dimer $((\mathbf{Rh_2})_3\mathbf{L_2})_2$ at $C = 10^{-3}$ M results in its complete dissociation into monomer $(\mathbf{Rh_2})_3\mathbf{L_2}$ (Figure S42). This transformation is monitored by the appearance of a characteristic ^{1}H NMR resonance at $\delta = 8.37$ ppm, assigned to the α-protons of the pyridine motifs, and is further confirmed by complementary ^{1}H DOSY NMR analysis (Figure S43). This confirms the reversible structural conversion occurring between the monomeric and dimeric cages in solution, through simple control over the concentration.

Guest-Induced Dissociation of the Dimeric Interlocked Cages $((Rh_2)_3L_2)_2$ into $2L\subset(Rh_2)_3L_2$

The dissociation of the interlocked dimer could also be operated through a guest binding process. When two equivalents of **L** were added per $(\mathbf{Rh_2})_3\mathbf{L_2}$ cage at $C = 2 \times 10^{-2}$ M (nitromethane-d_3—acetonitrile-d_3 (1/1 v/v)), i.e., exactly the concentration at which the interlocked cage exists as a unique species (Figure 6c), the system undergoes a clean transformation. After 1.5 h at 50 °C, the resulting ^{1}H NMR spectrum appears identical to that observed for of $\mathbf{2L}\subset(\mathbf{Rh_2})_3\mathbf{L_2}$, with no detectable traces of $((\mathbf{Rh_2})_3\mathbf{L_2})_2$, indicating a complete dissociation of the interlocked structure and the concomitant binding of two **L** molecules in the cavity of $(\mathbf{Rh_2})_3\mathbf{L_2}$ (Figures S65−S67). This was confirmed by ^{1}H DOSY NMR showing the formation of a single species ($D = 2.6 \times 10^{-10}$ m^2 s^{-1}) and by ESI-FTICR with the exclusive detection of multicharged ions corresponding to $\mathbf{2L}\subset(\mathbf{Rh_2})_3\mathbf{L_2}$ (Figure S68). In contrast, similar experiments carried out in the presence of perylenediimide derivative **G** do not show any change in the ^{1}H NMR spectrum of $((\mathbf{Rh_2})_3\mathbf{L_2})_2$. This indicates that no dissociation of the interlocked cage occurs in this case, consistent with the above finding that the $(\mathbf{Rh_2})_3\mathbf{L_2}$ cage exhibits a stronger affinity for **L** than for **G**.

Guest Release and Uptake

The controlled release and uptake[79,80] processes of **L** and **G** guests with $(\mathbf{Rh_2})_3\mathbf{L_2}$ were studied using various external stimuli, namely, competitive binding, modulation of the concentration, and pH changes.

Concentration-Dependent Release of G from $2G\subset(Rh_2)_3L_2$

Given that **G** cannot dissociate interlocked cages $((\mathbf{Rh_2})_3\mathbf{L_2})_2$, we examined the behavior of $\mathbf{2G}\subset(\mathbf{Rh_2})_3\mathbf{L_2}$ at various concentrations. We hypothesized that increasing the concentration of the host−guest complex solution should trigger **G** ejection, thanks to a cage dimerization process. This was followed by ^{1}H NMR experiments at concentrations ranging from 10^{-3} M to 2×10^{-2} M in a 1:1 mixture of nitromethane-d_3 and acetonitrile-d_3 at 50 °C (Figures S54 and S55). At low concentrations, the spectral profile remains characteristic of $\mathbf{2G}\subset(\mathbf{Rh_2})_3\mathbf{L_2}$, in accordance with a stable encapsulation. However, at the highest concentration, the ^{1}H NMR spectrum is dominated by the characteristic signals of the interlocked dimer $((\mathbf{Rh_2})_3\mathbf{L_2})_2$, although a few additional minor signals are also observed, which may reflect the presence of minor aggregated species or intermediate assemblies. This establishes that the concentration-driven cage dimerization directly induces the release of **G**, providing a clear demonstration that guest binding and interlocked assembly compete in a predictable, stimulus-dependent manner. In contrast, increasing the concentration of $\mathbf{2L}\subset(\mathbf{Rh_2})_3\mathbf{L_2}$ under identical conditions does not lead to guest release or cage dimerization, highlighting the object-specific nature of the concentration-induced behavior observed for $\mathbf{2G}\subset(\mathbf{Rh_2})_3\mathbf{L_2}$.

pH-Mediated Release and Uptake of L from $2L\subset(Rh_2)_3L_2$

Among the stimuli enabling controlled guest releases and/or uptakes, pH modulation represents a promising approach. Nevertheless, the Brønsted basicity of pyridyl ligands can also promote undesired side reactions or cage degradation upon protonation.

https://doi.org/10.1021/jacsau.6c00216
JACS Au XXXX, XXX, XXX−XXX

Given that the $(Rh_2)_3L_2$ cage can selectively encapsulate two **L** substrates containing noncoordinated pyridine units, we investigated how protonation would affect the encapsulated guests. We hypothesized that the selective protonation of the noncoordinated pyridyl units of **L** substrates would result in their ejection from the cationic cavity, driven both by the increasing electrostatic repulsion and by disruption of the stabilizing N−π interactions with the phenazine panels. We conducted experiments in nitromethane-d_3 at $C = 10^{-3}$ M using trifluoromethanesulfonic acid (HOTf) as a proton source[29] (Figure 8). The addition of six equiv of HOTf to a

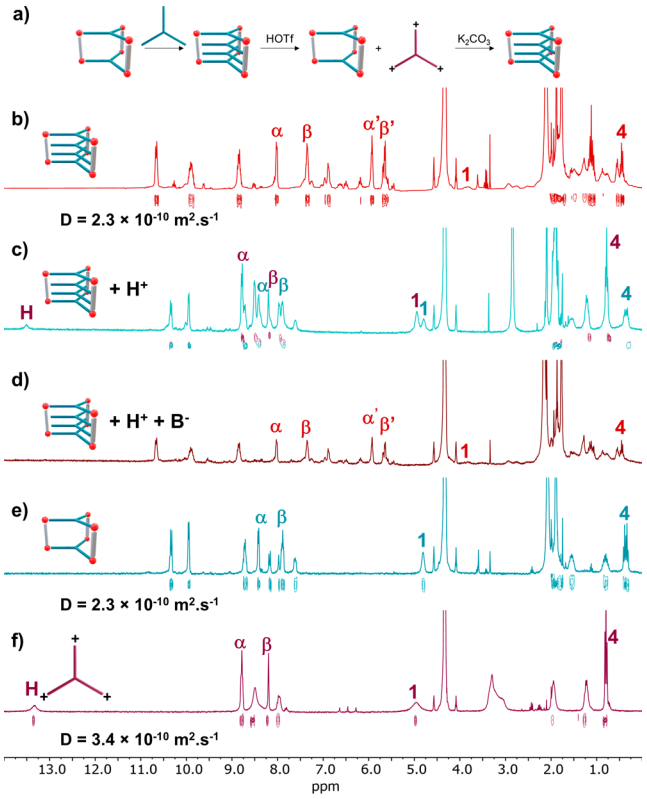

Figure 8. (a) Representation of the pH-mediated guest release/uptake and ^{1}H NMR spectra in nitromethane-d_3 at $C = 10^{-3}$ M (b) of **2L**⊂$(Rh_2)_3L_2$, (c) after addition of 6 equiv of HOTf (H^+) to **2L**⊂$(Rh_2)_3L_2$, (d) after addition of 6 equiv of K_2CO_3 (B^-) to (c), (e) of cage $(Rh_2)_3L_2$, and (f) after the addition of 3 equiv of HOTf to the ligand **L**. Primed labels (′) correspond to protons of the encapsulated guest, whereas unprimed labels correspond to protons of the cage framework.

solution of **2L**⊂$(Rh_2)_3L_2$ results in the appearance of new sets of signals in the ^{1}H NMR spectrum (Figure 8c) which are assigned to $(Rh_2)_3L_2$ (Figure 8e) and LH_3^{3+} species (Figures 8f and S13). Expulsion of the **L** substrates was further confirmed by ^{1}H DOSY NMR, which reveals two distinct species with diffusion coefficients of $D = 2.3 \times 10^{-10}$ m^2 s^{-1} and $D = 3.4 \times 10^{-10}$ m^2 s^{-1}, corresponding to $(Rh_2)_3L_2$ and LH_3^{3+}, respectively, as well as by ESI-FTICR mass spectrometry measurement which indicates the exclusive presence of $(Rh_2)_3L_2$ (Figures S45−S48).

Remarkably, the double guest release process proved to be reversible, as the addition of K_2CO_3 to the solution restores the **2L**⊂$(Rh_2)_3L_2$ complex, as confirmed by ^{1}H NMR (Figures 8d and S49−S51) and ESI-FTICR mass spectrometry (Figure S52).

pH-Mediated Guest Exchange in $(Rh_2)_3L_2$

The pH modulation could also be used to control the competitive guest exchange between **L** and **G** (Figure 9a). As

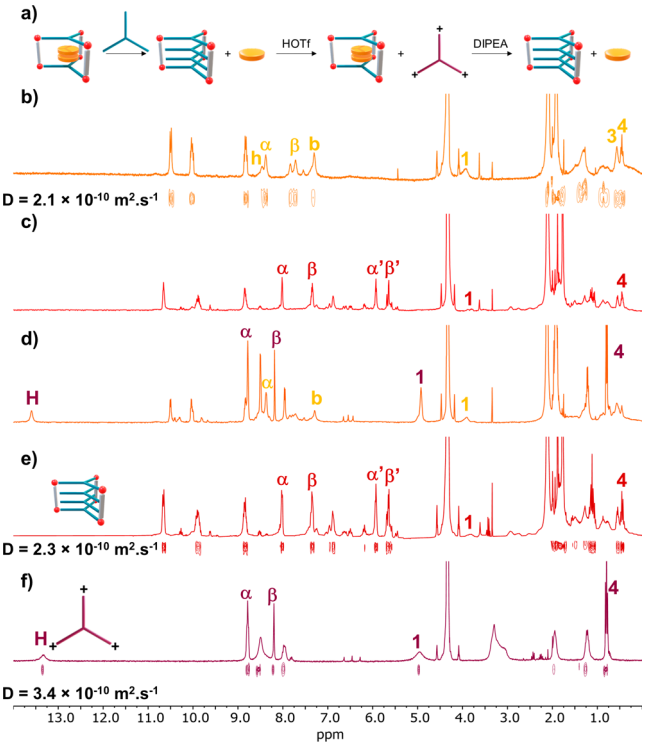

Figure 9. (a) Representation of the pH-mediated guest exchange and ^{1}H NMR in nitromethane at $C = 10^{-3}$ M (b) of cage **2G**⊂$(Rh_2)_3L_2$, (c) after addition of two equiv of **L** to **2G**⊂$(Rh_2)_3L_2$, (d) after addition of 6 equiv of HOTf to (c), (e) of cage **2G**⊂$(Rh_2)_3L_2$, and (f) after addition of 3 equiv of HOTf to the ligand **L**. Diagnostic signals for $(Rh_2)_3L_2$ and $((Rh_2)_3L_2)_2$) in (b) are indicated above the spectra using schematic representations of the corresponding species. Primed labels (′) correspond to protons of the encapsulated guest, whereas unprimed labels correspond to protons of the cage framework.

established above, the $(Rh_2)_3L_2$ cage exhibits a stronger binding affinity for compound **L** than **G**, indicating that **L** could potentially displace **G** from the host cavity. Accordingly, we added two equiv of compound **L** to a solution of **2G**⊂$(Rh_2)_3L_2$ in nitromethane-d_3. This led to a complete displacement of both **G** molecules and to the formation of **2L**⊂$(Rh_2)_3L_2$, an outcome confirmed by both ^{1}H NMR (Figures 9b,c, S57, and S58) and ESI-FTICR mass spectrometry analyses (Figure S59).

Treatment of this mixture with HOTf selectively protonates the pyridine units of the two encapsulated **L** guests, triggering their expulsion from the cavity and enabling the subsequent re-encapsulation of two **G** substrates, as confirmed by ^{1}H NMR (Figures 9d, S60, and S61) and ESI-FTICR mass spectrometry (Figure S62). Interestingly, the addition of six equiv of diisopropylethylamine (DIPEA) promoted the re-encapsulation of **L**, as again confirmed by ESI-FTICR mass spectrometry (Figure S63). These results demonstrate a fully reversible, pH-controlled **L**/**G** guest exchange cycle, in which protonation and deprotonation events selectively modulate cavity occupancy.

https://doi.org/10.1021/jacsau.6c00216
JACS Au XXXX, XXX, XXX−XXX

pH-Mediated Interconversion between $((Rh_2)_3L_2)_2$ and $2L\subset(Rh_2)_3L_2$

Finally, the behavior of $\mathbf{2L\subset(Rh_2)_3L_2}$ with pH was examined at a higher concentration (2×10^{-2} M) in a 1:1 mixture of nitromethane-d_3 and acetonitrile-d_3 (Figure 10a). At this concentration, releasing the guest molecule **L** from $\mathbf{2L\subset(Rh_2)_3L_2}$ is expected to promote the formation of the interlocked species $\mathbf{((Rh_2)_3L_2)_2}$. This was achieved upon addition of six equivalents of HOTf to a solution of $\mathbf{2L\subset(Rh_2)_3L_2}$. Both ^{1}H NMR spectroscopy (Figures 10d, S69, and S70) and ESI-FTICR mass spectrometry (Figure S71) confirm the exclusive formation of the interlocked $\mathbf{((Rh_2)_3L_2)_2}$ system, subsequently to the release of the two encapsulated guests. It is worth noting that the guest release proved to be reversible since addition of DIPEA restores $\mathbf{2L\subset(Rh_2)_3L_2}$ as shown by mass spectrometry (Figure S72). These observations reveal an unprecedented level of reversible control over the cage dimerization process: the protonation triggers a concerted release of the guest pair, which is replaced by the formation of the interlocked dimer, whereas the deprotonation restores the original host–guest complex. This behavior highlights the ability of this system to translate a simple acid–base stimulus into large-scale structural reorganization.

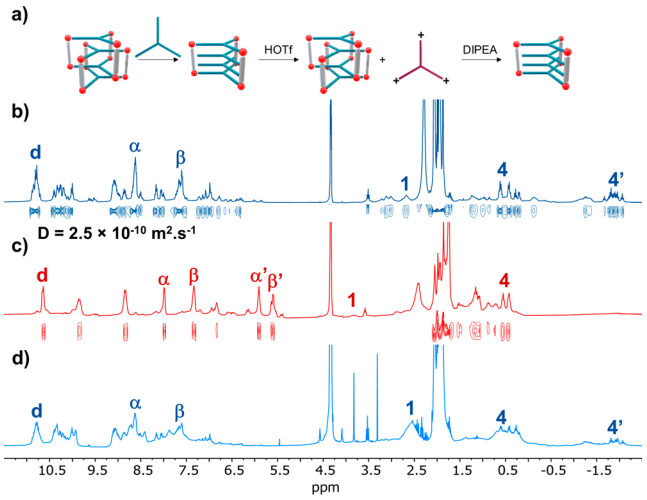

Figure 10. (a) Representation of the interconversion between the interlocked cages $\mathbf{((Rh_2)_3L_2)_2}$ and the cage $\mathbf{2L\subset(Rh_2)_3L_2}$ and ^{1}H NMR spectra in a nitromethane/acetonitrile at C = 2×10^{-2} M (b) of the interlocked cages $\mathbf{((Rh_2)_3L_2)_2}$, (c) after the addition of 4 equiv of **L** to a solution of $\mathbf{((Rh_2)_3L_2)_2}$, and (d) after the addition of 6 equiv of HOTf to a solution of (c). Primed labels (′) correspond to protons of the encapsulated guest, whereas unprimed labels correspond to protons of the cage framework.

CONCLUSION

In this work, we have carefully designed the original polyhedral cage $\mathbf{(Rh_2)_3L_2}$ and thoroughly investigated its unprecedented multifaceted supramolecular behavior. The latter is manifested by a versatile yet fully controlled access to four discrete, structurally characterized states, i.e., a monomeric cage, two distinct host–guest complexes, and a mechanically interlocked cage dimer, each of them being formed cleanly and selectively.

This level of structural control enables a series of interconnected supramolecular transformations that, taken together, are unprecedented in the case of coordination cages. The solution concentration dictates a fully reversible cage monomer to interlocked cage dimer transition. Guest substrates can dissociate or prevent cage dimer formation depending on their respective affinity, establishing a direct competition between guest encapsulation and establishing a higher-order interlocked assembly. Protonation triggers a concerted guest-pair release, a process that can be reversed upon deprotonation; remarkably, this acid–base stimulus also governs the pH-mediated conversion between a host–guest complex and an interlocked cage dimer at a high concentration. Finally, the system supports a fully reversible **L**/**G** guest exchange cycle.

While catenated cages, pH-responsive hosts, and guest-induced transformations have each been explored individually, their integration into a single, modular, reversible, and stimulus-responsive platform has not been demonstrated previously. In this system, mechanical interlocking, competitive guest binding, concentration-dependent structural reorganization, and pH-responsive switching operate in a fully integrated and reversible manner, allowing for programmed navigation between multiple well-defined architectures. The structural versatility of this multifaceted system, combined with the simplicity of the input driving interconversion, opens new avenues for the design of adaptive and multifunctional supramolecular architectures.

ASSOCIATED CONTENT

Supporting Information

The Supporting Information is available free of charge at https://pubs.acs.org/doi/10.1021/jacsau.6c00216.

Experimental procedures, spectroscopic data, computational methods, and X-ray crystallographic detail (PDF)

Accession Codes

Deposition numbers 2474817–2474820 contain the supplementary crystallographic data for this paper. These data can be obtained free of charge via the joint Cambridge Crystallographic Data Centre (CCDC) and Fachinformationszentrum Karlsruhe Access Structures service.

AUTHOR INFORMATION

Corresponding Authors

Luca Pesce – *University of Applied Sciences and Arts of Southern Switzerland, CH-6962 Lugano, Switzerland; Nantes Université, CNRS, F-44000 Nantes, France;* orcid.org/0000-0001-6364-9577; Email: Luca.Pesce@supsi.ch

Denis Jacquemin – *Nantes Université, CNRS, F-44000 Nantes, France; Institut Universitaire de France (IUF), F-75005 Paris, France;* orcid.org/0000-0002-4217-0708; Email: Denis.Jacquemin@univ-nantes.fr

Marc Sallé – *Univ Angers, CNRS, MOLTECH-ANJOU, F-49000 Angers, France; Nantes Université, CNRS, F-44000 Nantes, France;* orcid.org/0000-0003-4601-6334; Email: marc.salle@univ-angers.fr

Sébastien Goeb – *Univ Angers, CNRS, MOLTECH-ANJOU, F-49000 Angers, France;* orcid.org/0000-0003-2470-0768; Email: sebastien.goeb@univ-angers.fr

Authors

Romain Guechaichia – *Univ Angers, CNRS, MOLTECH-ANJOU, F-49000 Angers, France*

https://doi.org/10.1021/jacsau.6c00216
JACS Au XXXX, XXX, XXX–XXX

Amina Benchohra − *Univ Angers, CNRS, MOLTECH-ANJOU, F-49000 Angers, France; Laboratoire CEMCA UMR-CNRS 6521, Université de Bretagne Occidentale, F-29200 Brest, France;* orcid.org/0000-0002-6060-6894
Liam Miller − *Univ Angers, CNRS, MOLTECH-ANJOU, F-49000 Angers, France*
Jennifer Bou Zeid − *Univ Angers, CNRS, MOLTECH-ANJOU, F-49000 Angers, France*
David Canevet − *Univ Angers, CNRS, MOLTECH-ANJOU, F-49000 Angers, France*
Magali Allain − *Univ Angers, CNRS, MOLTECH-ANJOU, F-49000 Angers, France*
Vincent Carré − *Université de Lorraine, F-57000 Metz, France;* orcid.org/0000-0002-0719-7366
Frédéric Aubriet − *Université de Lorraine, F-57000 Metz, France;* orcid.org/0000-0003-2457-7974

Complete contact information is available at: https://pubs.acs.org/10.1021/jacsau.6c00216

Author Contributions

The manuscript was written through contributions of all authors. All authors have given approval to the final version of the manuscript.

Notes

The authors declare no competing financial interest.

■ ACKNOWLEDGMENTS

The authors gratefully acknowledge the Agence Nationale de la Recherche (ANR-21-CE06-0028 PoDACC) for a PhD grant (Romain Guechaichia) and a Postdoctoral fellowship (Luca Pesce), the EUR LUMOMAT project and the "Investissements d'Avenir" program ANR-18-EURE-0012 for a Postdoctoral fellowship (Amina Benchohra), and the University of Angers for a PhD grant (Jennifer Bou Zeid). They also acknowledge the ASTRAL (Benjamin Siegler for NMR spectroscopy) and CRISTAL platforms (SFR MATRIX, Univ. Angers) for their assistance in spectroscopic analyses. Financial support from IR INFRANALYTICS FR2054 for conducting ESI FT-ICR MS measurements at the facility in Metz (LCP-A2MC) is gratefully acknowledged. This work was further supported by the CNRS RECIPROCS network and was granted synchrotron beamtime by the SOLEIL scientific proposal committee (BAG proposal no. 20201238). The authors gratefully acknowledge Dr. Pierre Fertey for his assistance at the CRISTAL beamline. This work used the HPC resources from the GLiCID Computing Facility (Ligerien Group for Intensive Distributed Computing, 10.60487/glicid, Pays de la Loire, France).

■ REFERENCES

(1) Zhu, H.; Speakman, N. M. A.; Ronson, T. K.; Nitschke, J. R. Higher-Order Cu(I)-Based Cages via Subcomponent Self-Assembly. *Acc. Chem. Res.* **2025**, *58*, 1296−1307.
(2) Zhou, Y.; Yang, J.; Jie, K. Macrocyclic arene-based metal-organic cages. *Coord. Chem. Rev.* **2025**, *539*, 216726.
(3) Thoonen, S.; Tuck, K. L.; Turner, D. R. Discrete metallosupramolecular architectures with amino acids. *Coord. Chem. Rev.* **2025**, *522*, 216203.
(4) Xu, Z.; Ye, Y.; Liu, Y.; Liu, H.; Jiang, S. Design and assembly of porous organic cages. *Chem. Commun.* **2024**, *60*, 2261−2282.
(5) Moree, L. K.; Faulkner, L. A. V.; Crowley, J. D. Heterometallic cages: synthesis and applications. *Chem. Soc. Rev.* **2024**, *53*, 25−46.
(6) Cox, C. J. T.; Hale, J.; Molinska, P.; Lewis, J. E. M. Supramolecular and molecular capsules, cages and containers. *Chem. Soc. Rev.* **2024**, *53*, 10380−10408.
(7) Zhu, X.-W.; Luo, D.; Zhou, X.-P.; Li, D. Imidazole-based metal-organic cages: Synthesis, structures, and functions. *Coord. Chem. Rev.* **2022**, *455*, 214354.
(8) Liu, Y.; Huang, L.; Qin, L.; Zhou, T. Metal-Organic Cages: Synthetic Strategies and Photocatalytic Application. *ChemCatChem* **2024**, *17*, No. e202401487.
(9) Hao, Y.; Lu, Y. L.; Jiao, Z.; Su, C. Y. Photocatalysis Meets Confinement: An Emerging Opportunity for Photoinduced Organic Transformations. *Angew. Chem., Int. Ed.* **2024**, *63*, No. e202317808.
(10) Ashbridge, Z.; Reek, J. N. H. The multifaceted roles of MnL_2n cages in catalysis. *Nat. Synth.* **2024**, *3*, 1197−1207.
(11) Peng, Y.; Su, Z.; Jin, M.; Zhu, L.; Guan, Z. J.; Fang, Y. Recent advances in porous molecular cages for photocatalytic organic conversions. *Dalton Trans.* **2023**, *52*, 15216−15232.
(12) Chen, S.; Chen, L.-J. Metal−Organic Cages: Applications in Organic Reactions. *Chem.—Eur. J.* **2022**, *4*, 494−519.
(13) Zeng, Q. W.; Hu, L.; Niu, Y.; Wang, D.; Kang, Y.; Jia, H.; Dou, W. T.; Xu, L. Metal-organic cages for gas adsorption and separation. *Chem. Commun.* **2024**, *60*, 3469−3483.
(14) Banerjee, R.; Chakraborty, D.; Mukherjee, P. S. Molecular Barrels as Potential Hosts: From Synthesis to Applications. *J. Am. Chem. Soc.* **2023**, *145*, 7692−7711.
(15) Zhang, D.; Ronson, T. K.; Zou, Y. Q.; Nitschke, J. R. Metal-organic cages for molecular separations. *Nat. Rev. Chem.* **2021**, *5*, 168−182.
(16) Zhang, J. H.; Xie, S. M.; Zi, M.; Yuan, L. M. Recent advances of application of porous molecular cages for enantioselective recognition and separation. *J. Sep. Sci.* **2020**, *43*, 134−149.
(17) Wang, Y.-P.; Zhang, Y.; Duan, X.-H.; Mao, J.-J.; Pan, M.; Shen, J.; Su, C.-Y. Recent progress in metal-organic cages for biomedical application: Highlighted research during 2018−2023. *Coord. Chem. Rev.* **2024**, *501*, 215570.
(18) Monta-Gonzalez, G.; Ortiz-Gomez, E.; Lopez-Lima, R.; Fiorini, G.; Martinez-Manez, R.; Marti-Centelles, V. Water-Soluble Molecular Cages for Biological Applications. *Molecules* **2024**, *29*, 1621.
(19) Tapia, L.; Alfonso, I.; Sola, J. Molecular cages for biological applications. *Org. Biomol. Chem.* **2021**, *19*, 9527−9540.
(20) Zhao, J.; Zhang, Y.; Wang, Z.; Yang, D. Incorporation of Cages into Gels: Access to a New Class of Soft Materials with Well-Defined Functionality. *Chem.—Eur. J.* **2025**, *31*, No. e202404363.
(21) Drozdz, W.; Ciesielski, A.; Stefankiewicz, A. R. Dynamic Cages-Towards Nanostructured Smart Materials. *Angew. Chem., Int. Ed.* **2023**, *62*, No. e202307552.
(22) Benchimol, E.; Tessarolo, J.; Clever, G. H. Photoswitchable coordination cages. *Nat. Chem.* **2024**, *16*, 13−21.
(23) Lin, H. Y.; Wang, Y. T.; Shi, X.; Yang, H. B.; Xu, L. Switchable metallacycles and metallacages. *Chem. Soc. Rev.* **2023**, *52*, 1129−1154.
(24) Benchimol, E.; Nguyen, B. T.; Ronson, T. K.; Nitschke, J. R. Transformation networks of metal-organic cages controlled by chemical stimuli. *Chem. Soc. Rev.* **2022**, *51*, 5101−5135.
(25) Percástegui, E. G. Guest-Induced Transformations in Metal-Organic Cages. *Eur. J. Inorg. Chem.* **2021**, *2021*, 4425−4438.
(26) Wezenberg, S. J. Light-switchable Metal-Organic Cages. *Chem. Lett.* **2020**, *49*, 609−615.
(27) Blanco-Gomez, A.; Corton, P.; Barravecchia, L.; Neira, I.; Pazos, E.; Peinador, C.; Garcia, M. D. Controlled binding of organic guests by stimuli-responsive macrocycles. *Chem. Soc. Rev.* **2020**, *49*, 3834−3862.
(28) Chen, L. J.; Yang, H. B. Construction of Stimuli-Responsive Functional Materials via Hierarchical Self-Assembly Involving Coordination Interactions. *Acc. Chem. Res.* **2018**, *51*, 2699−2710.
(29) Dekhtiarenko, M.; Pascal, S.; Elhabiri, M.; Mazan, V.; Canevet, D.; Allain, M.; Carré, V.; Aubriet, F.; Voitenko, Z.; Sallé, M.; Siri, O.; Goeb, S. Reversible pH-Controlled Catenation of a Benzobisimidazole-Based Tetranuclear Rectangle. *Chem.—Eur. J.* **2021**, *27*, 15922−15927.

(30) Lisboa, L. S.; Findlay, J. A.; Wright, L. J.; Hartinger, C. G.; Crowley, J. D. A Reduced-Symmetry Heterobimetallic $[PdPtL_4]^{4+}$ Cage: Assembly, Guest Binding, and Stimulus-Induced Switching. *Angew. Chem., Int. Ed.* **2020**, *59*, 11101−11107.
(31) Jansze, S. M.; Severin, K. Palladium-Based Metal-Ligand Assemblies: The Contrasting Behavior upon Addition of Pyridine or Acid. *J. Am. Chem. Soc.* **2019**, *141*, 815−819.
(32) Szaloki, G.; Croué, V.; Carré, V.; Aubriet, F.; Alévêque, O.; Levillain, E.; Allain, M.; Arago, J.; Orti, E.; Goeb, S.; Sallé, M. Controlling the Host-Guest Interaction Mode through a Redox Stimulus. *Angew. Chem., Int. Ed.* **2017**, *56*, 16272−16276.
(33) Croué, V.; Goeb, S.; Szaloki, G.; Allain, M.; Sallé, M. Reversible Guest Uptake/Release by Redox-Controlled Assembly/Disassembly of a Coordination Cage. *Angew. Chem., Int. Ed.* **2016**, *55*, 1746−1750.
(34) Mansoor, I. F.; Dutton, K. G.; Rothschild, D. A.; Remsing, R. C.; Lipke, M. C. Uptake, Trapping, and Release of Organometallic Cations by Redox-Active Cationic Hosts. *J. Am. Chem. Soc.* **2021**, *143*, 16993−17003.
(35) Szaloki, G.; Krykun, S.; Croué, V.; Allain, M.; Morille, Y.; Aubriet, F.; Carré, V.; Voitenko, Z.; Goeb, S.; Sallé, M. Redox-Driven Transformation of a Discrete Molecular Cage into an Infinite 3D Coordination Polymer. *Chem.—Eur. J.* **2018**, *24*, 11273−11277.
(36) Freye, S.; Michel, R.; Stalke, D.; Pawliczek, M.; Frauendorf, H.; Clever, G. H. Template control over dimerization and guest selectivity of interpenetrated coordination cages. *J. Am. Chem. Soc.* **2013**, *135*, 8476−8479.
(37) Zhu, R.; Regeni, I.; Holstein, J. J.; Dittrich, B.; Simon, M.; Prevost, S.; Gradzielski, M.; Clever, G. H. Catenation and Aggregation of Multi-Cavity Coordination Cages. *Angew. Chem., Int. Ed.* **2018**, *57*, 13652−13656.
(38) Yang, L.; Jing, X.; An, B.; He, C.; Yang, Y.; Duan, C. Binding of anions in triply interlocked coordination catenanes and dynamic allostery for dehalogenation reactions. *Chem. Sci.* **2018**, *9*, 1050−1057.
(39) Cheng, P. M.; Cai, L. X.; Li, S. C.; Hu, S. J.; Yan, D. N.; Zhou, L. P.; Sun, Q. F. Guest-Reaction Driven Cage to Conjoined Twin-Cage Mitosis-Like Host Transformation. *Angew. Chem., Int. Ed.* **2020**, *59*, 23569−23573.
(40) Domoto, Y.; Abe, M.; Fujita, M. A Highly Entangled $(M_3L_2)_8$ Truncated Cube from the Anion-Controlled Oligomerization of a pi-Coordinated M_3L_2 Subunit. *J. Am. Chem. Soc.* **2021**, *143*, 8578−8582.
(41) Hugenbusch, D.; Lehr, M.; von Glasenapp, J. S.; McConnell, A. J.; Herges, R. Light-Controlled Destruction and Assembly: Switching between Two Differently Composed Cage-Type Complexes. *Angew. Chem., Int. Ed.* **2023**, *62*, No. e202212571.
(42) Oldknow, S.; Martir, D. R.; Pritchard, V. E.; Blitz, M. A.; Fishwick, C. W. G.; Zysman-Colman, E.; Hardie, M. J. Structure-switching M_3L_2 Ir(III) coordination cages with photo-isomerising azo-aromatic linkers. *Chem. Sci.* **2018**, *9*, 8150−8159.
(43) Guo, S.; Li, M.; Hu, H.; Xu, T.; Xi, H.; Zhu, W. H. Light-regulating chirality of metallacages featuring dithienylethene switches. *Chem. Sci.* **2023**, *14*, 6237−6243.
(44) Jansze, S. M.; Cecot, G.; Severin, K. Reversible disassembly of metallasupramolecular structures mediated by a metastable-state photoacid. *Chem. Sci.* **2018**, *9*, 4253−4257.
(45) Fu, S.; Luo, Q.; Zang, M.; Tian, J.; Zhang, Z.; Zeng, M.; Ji, Y.; Xu, J.; Liu, J. Light-triggered reversible disassembly of stimuli-responsive coordination metallosupramolecular Pd2L4 cages mediated by azobenzene-containing ligands. *Mater. Chem. Front.* **2019**, *3*, 1238−1243.
(46) Xie, T. Z.; Endres, K. J.; Guo, Z.; Ludlow, J. M., 3rd; Moorefield, C. N.; Saunders, M. J.; Wesdemiotis, C.; Newkome, G. R. Controlled Interconversion of Superposed-Bistriangle, Octahedron, and Cuboctahedron Cages Constructed Using a Single, Terpyridinyl-Based Polyligand and Zn(II). *J. Am. Chem. Soc.* **2016**, *138*, 12344−12347.
(47) Davies, J. A.; Ronson, T. K.; Nitschke, J. R. Twisted rectangular subunits self-assemble into a ferritin-like capsule. *Chem* **2022**, *8*, 1099−1106.
(48) Kilbas, B.; Mirtschin, S.; Scopelliti, R.; Severin, K. A solvent-responsive coordination cage. *Chem. Sci.* **2012**, *3*, 701−704.
(49) Matsumoto, K.; Kusaba, S.; Tanaka, Y.; Sei, Y.; Akita, M.; Aritani, K.; Haga, M. A.; Yoshizawa, M. A Peanut-Shaped Polyaromatic Capsule: Solvent-Dependent Transformation and Electronic Properties of a Non-Contacted Fullerene Dimer. *Angew. Chem., Int. Ed.* **2019**, *58*, 8463−8467.
(50) Cai, L. X.; Yan, D. N.; Cheng, P. M.; Xuan, J. J.; Li, S. C.; Zhou, L. P.; Tian, C. B.; Sun, Q. F. Controlled Self-Assembly and Multistimuli-Responsive Interconversions of Three Conjoined Twin-Cages. *J. Am. Chem. Soc.* **2021**, *143*, 2016−2024.
(51) Edo-Osagie, A.; Serillon, D.; Ruani, F.; Barril, X.; Gourlaouen, C.; Armaroli, N.; Ventura, B.; Jacquot de Rouville, H. P.; Heitz, V. Multi-Responsive Eight-State Bis(acridinium-Zn(II) porphyrin) Receptor. *J. Am. Chem. Soc.* **2023**, *145*, 10691−10699.
(52) Endo, K.; Ube, H.; Shionoya, M. Multi-Stimuli-Responsive Interconversion between Bowl- and Capsule-Shaped Self-Assembled Zinc(II) Complexes. *J. Am. Chem. Soc.* **2020**, *142*, 407−416.
(53) Hou, H.; Jiang, Z.; Chen, Q.; Sun, Q.-F.; Hong, M. A Conformation-Adaptive Coordination Host: From Multi-Stimuli-Responsive Deformations to Regulating Guest Reactivity. *CCS Chem.* **2026**, *8*, 1106−1121.
(54) Li, R. J.; Tessarolo, J.; Lee, H.; Clever, G. H. Multi-stimuli Control over Assembly and Guest Binding in Metallo-supramolecular Hosts Based on Dithienylethene Photoswitches. *J. Am. Chem. Soc.* **2021**, *143*, 3865−3873.
(55) Yang, Y. C.; Ronson, T. K.; Teeuwen, P. C. P.; Du, Y. Y.; Zheng, J. Y.; Wales, D. J.; Nitschke, J. R. Guest binding is governed by multiple stimuli in low-symmetry metal-organic cages containing bis-pyridyl(imine) vertices. *Chem* **2025**, *11*, 102288.
(56) Zhang, H. N.; Yu, W. B.; Lin, Y. J.; Jin, G. X. Stimuli-Responsive Topological Transformation of a Molecular Borromean Ring via Controlled Oxidation of Thioether Moieties. *Angew. Chem., Int. Ed.* **2021**, *60*, 15466−15471.
(57) Zhang, Z.; Bai, Q.; Zhai, Z.; Long, Q.; Han, E.; Zhao, H.; Zhou, C. W.; Lin, H.; Zhang, W.; Ning, G. H.; Xie, T. Z.; Wang, P.; Wu, T. Multiple-stimuli fluorescent responsive metallo-organic helicated cage arising from monomer and excimer emission. *Nat. Commun.* **2024**, *15*, 7261.
(58) Hardy, M.; Struch, N.; Holstein, J. J.; Schnakenburg, G.; Wagner, N.; Engeser, M.; Beck, J.; Clever, G. H.; Lutzen, A. Dynamic Complex-to-Complex Transformations of Heterobimetallic Systems Influence the Cage Structure or Spin State of Iron(II) Ions. *Angew. Chem., Int. Ed.* **2020**, *59*, 3195−3200.
(59) Riddell, I. A.; Ronson, T. K.; Clegg, J. K.; Wood, C. S.; Bilbeisi, R. A.; Nitschke, J. R. Cation- and anion-exchanges induce multiple distinct rearrangements within metallosupramolecular architectures. *J. Am. Chem. Soc.* **2014**, *136*, 9491−9498.
(60) Plajer, A. J.; Percastegui, E. G.; Santella, M.; Rizzuto, F. J.; Gan, Q.; Laursen, B. W.; Nitschke, J. R. Fluorometric Recognition of Nucleotides within a Water-Soluble Tetrahedral Capsule. *Angew. Chem., Int. Ed.* **2019**, *58*, 4200−4204.
(61) Wang, Y.; Zhang, Y.; Zhou, Z.; Vanderlinden, R. T.; Li, B.; Song, B.; Li, X.; Cui, L.; Li, J.; Jia, X.; Fang, J.; Li, C.; Stang, P. J. A cyclic bis[2]catenane metallacage. *Nat. Commun.* **2020**, *11*, 2727.
(62) Roberts, D. A.; Pilgrim, B. S.; Sirvinskaite, G.; Ronson, T. K.; Nitschke, J. R. Covalent Post-assembly Modification Triggers Multiple Structural Transformations of a Tetrazine-Edged Fe(4)L(6) Tetrahedron. *J. Am. Chem. Soc.* **2018**, *140*, 9616−9623.
(63) Zhang, Z.; Bai, Q.; Zhai, Z.; Long, Q.; Han, E.; Zhao, H.; Zhou, C. W.; Lin, H.; Zhang, W.; Ning, G. H.; Xie, T. Z.; Wang, P.; Wu, T. Multiple-stimuli fluorescent responsive metallo-organic helicated cage arising from monomer and excimer emission. *Nat. Commun.* **2024**, *15*, 7261.
(64) Yang, Y.; Ronson, T. K.; Teeuwen, P. C. P.; Du, Y.; Zheng, J.; Wales, D. J.; Nitschke, J. R. Guest binding is governed by multiple stimuli in low-symmetry metal-organic cages containing bis-pyridyl-(imine) vertices. *Chem* **2025**, *11*, 102288.

https://doi.org/10.1021/jacsau.6c00216
JACS Au XXXX, XXX, XXX−XXX

(65) He, X.; Man, V. H.; Yang, W.; Lee, T.-S.; Wang, J. A fast and high-quality charge model for the next generation general AMBER force field. *J. Chem. Phys.* **2020**, *153*, 114502.
(66) Invernizzi, M.; Parrinello, M. Rethinking Metadynamics: From Bias Potentials to Probability Distributions. *J. Phys. Chem. Lett.* **2020**, *11*, 2731−2736.
(67) Séjourné, S.; Labrunie, A.; Dalinot, C.; Benchohra, A.; Carré, V.; Aubriet, F.; Allain, M.; Sallé, M.; Goeb, S. Chiral Self-Sorting in Truxene-Based Metallacages. *Inorganics* **2020**, *8*, 1.
(68) Benchohra, A.; Séjourné, S.; Labrunie, A.; Miller, L.; Charbonneau, E.; Carré, V.; Aubriet, F.; Allain, M.; Sallé, M.; Goeb, S. Controlling Chiral Self-Sorting in Truxene-Based Self-Assembled Cages. *Inorganics* **2022**, *10*, 103.
(69) Séjourné, S.; Labrunie, A.; Dalinot, C.; Canevet, D.; Guechaichia, R.; Bou Zeid, J.; Benchohra, A.; Cauchy, T.; Brosseau, A.; Allain, M.; Chamignon, C.; Viger-Gravel, J.; Pintacuda, G.; Carré, V.; Aubriet, F.; Vanthuyne, N.; Sallé, M.; Goeb, S. Chiral Truxene-Based Self-Assembled Cages: Triple Interlocking and Supramolecular Chirogenesis. *Angew. Chem., Int. Ed.* **2024**, *63*, No. e202400961.
(70) Avram, L.; Cohen, Y. Diffusion NMR of molecular cages and capsules. *Chem. Soc. Rev.* **2015**, *44*, 586−602.
(71) Singh, S. K.; Das, A. The n → π^* interaction: a rapidly emerging non-covalent interaction. *Phys. Chem. Chem. Phys.* **2015**, *17*, 9596−9612.
(72) Marti-Rujas, J. Mechanical interlocking of metal organic cages. *Commun. Chem.* **2025**, *8*, 92.
(73) Du, E.; Tang, X.; Zhang, W.; Dong, J.; Cui, Y.; Liu, Y. Emerging mechanically interlocked cages. *Nat. Rev. Chem.* **2025**, *9*, 506−522.
(74) Greed, S. Picking an inter-locked cage. *Nat. Rev. Chem.* **2024**, *8*, 155.
(75) Zhu, R.; Ding, J.; Jin, L.; Pang, H. Interpenetrated structures appeared in supramolecular cages, MOFs, COFs. *Coord. Chem. Rev.* **2019**, *389*, 119−140.
(76) Huang, S.-L.; Hor, T. S. A.; Jin, G.-X. Metallacyclic assembly of interlocked superstructures. *Coord. Chem. Rev.* **2017**, *333*, 1−26.
(77) Frank, M.; Johnstone, M. D.; Clever, G. H. Interpenetrated Cage Structures. *Chem.—Eur. J.* **2016**, *22*, 14104−14125.
(78) The viscosity of the acetonitrile-d_3/nitromethane-d_3 (1:1 v/v) solvent mixture was determined experimentally using the monomeric $(\mathbf{Rh_2})_3\mathbf{L}_2$ cage as a reference of known hydrodynamic radius. This calculated viscosity of 0.433 mPa s at 298 K was then employed to estimate the hydrodynamic radius of the interlocked $((\mathbf{Rh_2})_3\mathbf{L}_2)_2$ assembly.
(79) Kim, T. Y.; Vasdev, R. A. S.; Preston, D.; Crowley, J. D. Strategies for Reversible Guest Uptake and Release from Metallosupramolecular Architectures. *Chem.—Eur. J.* **2018**, *24*, 14878−14890.
(80) Goeb, S.; Sallé, M. Electron-rich Coordination Receptors Based on Tetrathiafulvalene Derivatives: Controlling the Host-Guest Binding. *Acc. Chem. Res.* **2021**, *54*, 1043−1055.

https://doi.org/10.1021/jacsau.6c00216
JACS Au XXXX, XXX, XXX−XXX